Electronic Supplementary Information (ESI) for

Laboratory-scale photoredox catalysis using hydrated electrons sustainably generated with a single green laser

*By Robert Naumann, Christoph Kerzig and Martin Goez**

Contents

1 Comprehensive experimental details S1
1.1 General S1
1.2 Absorption spectra and concentration determinations of all key species . . . S2

2 Mechanistic details S3
2.1 OER formation through quenching of ^{3}MLCT by Asc^{2-} S3
2.2 Closed-form kinetic treatment of the catalytic cycle S4
2.3 Thermal reaction between Asc^{2-} and the irradiated catalyst S6

3 Application-related details S6
3.1 Electron capture by ClPhAcA S6

1 Comprehensive experimental details

1.1 General

All chemicals were obtained commercially in the highest available purity and used as received: tris(2,2'-bipyridyl)dichlororuthenium(II) hexahydrate, 99.95 %, Aldrich; (+)-sodium L-ascorbate, > 99 %, Aldrich; sodium hydroxide, 99 %, Aldrich; sodium chloroacetate, 98 %, Aldrich; 4-chlorobenzoic acid, 99 %, Aldrich; benzoic acid, > 99.5 %, Aldrich; 4-chlorophenylacetic acid, 99 %, Aldrich; phenylacetic acid, 99 %, Aldrich; 3,3-dimethyl-2-butanone, 98 %, Aldrich; sodium dodecyl sulfate, > 99.5 %, Carl Roth; disodium 1,5-naphthalenedisulfonate hydrate, > 98 %, TCI; deuterium oxide, 99.9 atom % D, Deutero; sulfuric acid, 98 %, Carl Roth.

Oxygen was removed by purging the solutions with N_2O or Argon (5.0, Air Liquide) for 45 min before and during all experiments.

Nanosecond laser flash photolysis experiments with optical detection of the intermediates were carried out with a setup described in Ref. 21 of the main paper. In short, a frequency doubled Nd:YAG laser (Continuum Surelite-III, 5 ns pulse width) was used for excitation with 532 nm, and transient absorption or luminescence was monitored at right angle to the excitation (optical path length, 4 mm). Unless otherwise indicated (as in Figure 4 of the main paper), the solutions were pumped through the suprasil observation cell to ensure that each trace was recorded on fresh solution.

*Prof. Dr. Martin Goez, Robert Naumann, Dr. Christoph Kerzig, Martin-Luther-Universität Halle-Wittenberg, Institut für Chemie, Kurt-Mothes-Str. 2, D-06120 Halle (Saale), Germany.
E-mail: martin.goez@chemie.uni-halle.de

For the measurements of the catalyst stability and the photoredox catalysis experiments (Sections 2.2 and 2.3 of the main paper), 3.8 mL of the degassed solutions were transferred to a fluorescence cuvette (1 cm×1 cm×4 cm) and irradiated, under continuous stirring, with the laser running at a repetition rate of 10 Hz. The illuminated volume was about 17 % of the initial solution volume; aliquots taken for analysis in Section 2.2 of the main paper were 0.25 ml. These aliquots were diluted to 3.75 ml and brought to pH 1 before measuring the luminescence, the former to avoid filter effects caused by the absorption at the excitation wavelength, the latter to avoid quenching by the ascorbate di- and monoanion.

The NMR product analysis was performed on a 400 MHz Varian 400 VNMRS spectrometer at room temperature. The PRESAT pulse sequence was employed to suppress the intense water signal. For workup of each sample after irradiation, 10 % v/v of D_2O was added for shimming and locking; the pH was adjusted to 1 with concentrated H_2SO_4 (except for the experiments on ClPhA and ClPhAcA); and for quantification of the product concentrations reference substances were added, namely, disodium 1,5-naphthalenedisulfonate hydrate (for the experiments on ClAcA and TBMK) or sodium dodecyl sulfate (for the experiments on ClPhA and ClPhAcA).

Steady-state absorption and luminescence spectra were recorded on a Shimadzu UV-1800 spectrophotometer and a Perkin-Elmer LS 50B fluorimeter.

1.2 Absorption spectra and concentration determinations of all key species

Supplementary Figure 1 gives the absorption spectra of the catalyst Rubpy in its ground state GS and its one-electron reduced form OER. Careful recalibration the OER spectrum (see, Ref. 12 of the main paper) against the phenoxy radical of 4-methoxy phenolate and against the one-electron reduced methylviologen radical both gave an extinction coefficient at 505 nm of 15, 700 $M^{-1}cm^{-1}$. The spectrum of the metal-to-ligand charge-transfer excited state ^{3}MLCT has not been included because this species is too short lived at the high quencher concentrations normally used in the experiments.

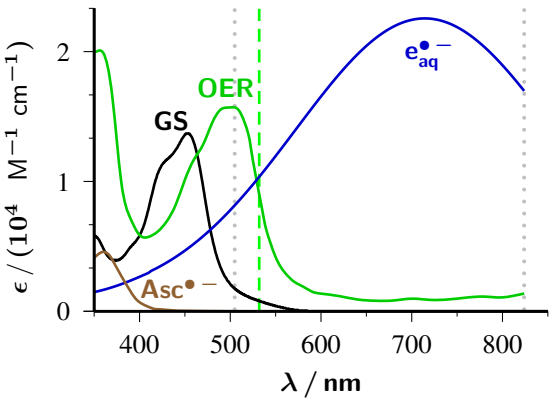

Supplementary Figure 1: Calibrated absorption spectra of all key species in the near-UV and visible ranges, corrected for ground-state depletion where applicable. The same colour codes and species abbreviations as in the main paper have been used. The dotted gray lines indicate the observation wavelengths for OER and $e^{\bullet}_{aq}{}^{-}$, the dashed green line the excitation wavelength of the laser. For further information, see text.

The spectrum of the quencher Asc^{2-} is also not shown, because it absorbs only marginally ($\varepsilon < 100\,M^{-1}cm^{-1}$, see Ref. 42 of the main paper) even at the left edge of the displayed spectral range. At our detection wavelengths, which lie above 500 nm, Asc^{2-} is completely

transparent, as is the quencher-derived radical $Asc^{\bullet-}$. The monoanion $AscH^-$ has no discernible absorption throughout in the wavelength range of Supplementary Figure 1.

For technical reasons we observed the hydrated electron $e_{aq}^{\bullet-}$ not at its absorption maximum but at 824 nm (extinction coefficient, 16,900 $M^{-1}cm^{-1}$). At that wavelength, an emission spike of the Xe lamp of our detection system leads to a much improved sensitivity. Details of the recording and calibration procedure of the spectrum can be found in Refs. 42 and 13 of the main paper.

At our monitoring wavelengths for $e_{aq}^{\bullet-}$ or OER the respective other species absorbs noticeably or even significantly. We circumvented this problem by recording (additional) traces in the same solutions saturated with N_2O. N_2O quantitatively transforms $e_{aq}^{\bullet-}$ into nonabsorbing hydroxyl radicals on a timescale similar to our laser pulses; and the hydroxyl radical are scavenged equally fast by Asc^{2-} (at the mM concentrations typically used) to give $Asc^{\bullet-}$(compare Ref. 14 of the main paper). Hence, in our time-resolved experiments the secondary chemistry is not influenced by the presence or absence of N_2O; detection at 824 nm in difference experiments without and with N_2O yields the pure electron traces, and detection at 505 nm under N_2O the pure OER traces.

2 Mechanistic details

2.1 OER formation through quenching of ^{3}MLCT by Asc^{2-}

To redetermine the quenching parameters of ^{3}MLCT by Asc^{2-} reported in Ref. 12 of the main paper, we performed Stern–Volmer experiments on Rubpy at room temperature, as displayed in Supplementary Figure 2. The Stern–Volmer plot (see, inset) is linear and gives a quenching rate constant of 5.1×10^9 $M^{-1}s^{-1}$, after correction for noneffective fraction of the quencher present as the monoanion $AscH^-$ at the experimental pH. OER is produced with the same rate, but not quantitatively; an analysis using the spectral data of Supplementary Figure 1 gives a value of 0.48 for the efficiency η of OER formation.

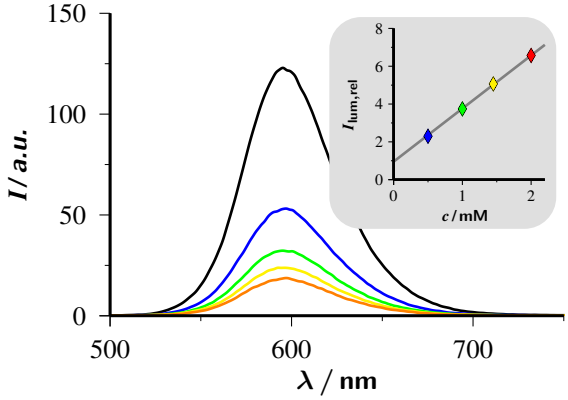

Supplementary Figure 2: Quenching of ^{3}MLCT by Asc^{2-}. Main plot, luminescence spectra (excitation wavelength, 455 nm) of an argon saturated 10 μM aqueous solution of Rubpy at pH 12.65 (100 mM NaOH) additionally containing 0 mM (black), 0.5 mM (blue), 1.0 mM (green), 1.5 mM (yellow) and 2.0 mM (orange) sodium ascorbate. Inset, corresponding Stern–Volmer plot; slope, 2.80/mM. For further information, see text.

2.2 Closed-form kinetic treatment of the catalytic cycle

For rectangular envelopes of the laser pulses, the intensity dependences shown in Figure 3a of the main paper can be described in closed form for the two limiting situations of short-lived (relative to the pulse duration) and long-lived spin-correlated radical pairs. In both these cases, the mechanism is reduced to that of Figure 1 of the main paper; together with the pertaining rate constants, this is displayed in Supplementary Figure 3.

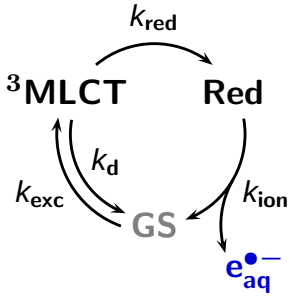

Supplementary Figure 3: Mechanism with the substance abbreviations and rate constants used for the kinetic treatment of this Section. For further explanation, see text.

In addition to the ground state GS and the excited state ^{3}MLCT the mechanistic scheme comprises only one reduced form Red of the catalyst. Red has to be identified with OER when ^{3}SCRP is short-lived, or with ^{3}SCRP when it is long-lived. The processes directly connecting GS and ^{3}MLCT are the same as in Figure 3b of the main paper, namely, excitation with rate constant k_{exc} and deactivation with rate constant τ^{-1} (hereafter denoted as k_d). Red is formed from ^{3}MLCT with rate constant k_{red} equalling $k_q\left[Asc^{2-}\right]$ times a constant, which is either η (short-lived ^{3}SCRP) or unity (long-lived ^{3}SCRP). Ionization with rate constant k_{ion} closes the cycle and liberates $e^{\bullet-}_{aq}$.

All the rate constants are (pseudo) first-order rate constants, with k_{exc} and k_{ion} additionally being proportional to the laser intensity. Because of the stoichiometric relationship $[GS] + \left[^3MLCT\right] + [Red] = c_0$, the kinetics of all species are thus biexponential, with the two characteristic constants k_+ and k_- given by

$$\begin{aligned} 2k_\pm =& k_{exc} + k_d + k_{red} + k_{ion} \\ & \pm \sqrt{(k_{exc} + k_d + k_{red} + k_{ion})^2 - 4\left[k_{exc}k_{red} + k_{ion}\left(k_{exc} + k_d + k_{red}\right)\right]} \end{aligned} \tag{S1}$$

The time-dependent concentrations of the two catalyst-derived species ^{3}MLCT and Red during the laser pulse are found to be

$$\begin{aligned} \frac{\left[^3MLCT\right]}{c_0} = \frac{k_{exc}k_{ion}}{k_+k_-}\Bigg\{1 &- \frac{k_+ + k_{red}k_{exc}/k_{ion} - k_{ion}}{k_+ - k_-}\exp(-k_+t) \\ &+ \frac{k_- + k_{red}k_{exc}/k_{ion} - k_{ion}}{k_+ - k_-}\exp(-k_-t)\Bigg\} \end{aligned} \tag{S2}$$

$$\frac{[Red]}{c_0} = \frac{k_{exc}k_{red}}{k_+k_-}\left\{1 + \frac{k_-}{k_+ - k_-}\exp(-k_+t) - \frac{k_+}{k_+ - k_-}\exp(-k_-t)\right\} \tag{S3}$$

Despite the fact that the square root in Supplementary Equation S1 can become complex,

the concentrations calculated with Supplementary Equations S2 and S3 are always real quantities, as they must.

The electron concentration follows from multiplying the concentration of Red with k_{ion} and integrating over the pulse (duration, T),

$$\frac{\left[\mathrm{e}_{\mathrm{aq}}^{\bullet-}\right]}{c_0} = \frac{k_{\mathrm{exc}}k_{\mathrm{red}}}{k_+k_-}k_{\mathrm{ion}}\frac{k_+ + k_-}{k_+k_-}\left\{\frac{k_+k_-}{k_+ + k_-}T - 1 - \frac{k_-^2}{k_+^2 - k_-^2}\exp(-k_+T) + \frac{k_+^2}{k_+^2 - k_-^2}\exp(-k_-T)\right\} \tag{S4}$$

The observable [OER] is obtained by multiplying the end-of-pulse concentration of ^{3}MLCT (Supplementary Equation S2) with the product of the Stern–Volmer factor $k_{\mathrm{red}}/(k_{\mathrm{red}} + k_{\mathrm{d}})$ and η, and adding to this the end-of-pulse concentration of Red (Supplementary Equation S3) weighted with either unity (short-lived ^{3}SCRP) or η (long-lived ^{3}SCRP).

The product k_+k_- equals the term in square brackets within the root in Supplementary Equation S1. Because in our strongly quenched samples k_{d} can be neglected against k_{red} and because $k_{\mathrm{ion}} \ll k_{\mathrm{exc}}$, the asymptotic limits of Supplementary Equations S2 and S3 are approximately given by $k_{\mathrm{ion}}/(k_{\mathrm{red}} + k_{\mathrm{ion}})$ and $k_{\mathrm{red}}/(k_{\mathrm{red}} + k_{\mathrm{ion}})$, respectively. The calculation outlined in the preceding paragraph thus leads to plateau values of OER that are $\left(k_{\mathrm{ion}} + k_{\mathrm{q}}\left[\mathrm{Asc}^{2-}\right]\right) / \left(k_{\mathrm{ion}}/\eta + k_{\mathrm{q}}\left[\mathrm{Asc}^{2-}\right]\right)$ (short-lived ^{3}SCRP) and η (long-lived ^{3}SCRP); in strongly quenched samples, the former approaches unity whereas the latter remains at η.

On these grounds, the experimental results cannot be reconciled with ^{3}SCRP being short-lived. This is borne out by the best fit of Supplementary Figure 4a, which represents the data very poorly. The assumption of long-lived ^{3}SCRP accommodates the data much better, although in Supplementary Figure 4b some systematic deviations are evident for OER in the region of low Asc^{2-} concentrations. A practically perfect fit is obtained with the numerical solution (see, Figure 3a of the main paper) for the case that ^{3}SCRP lives only slightly longer than the pulse duration.

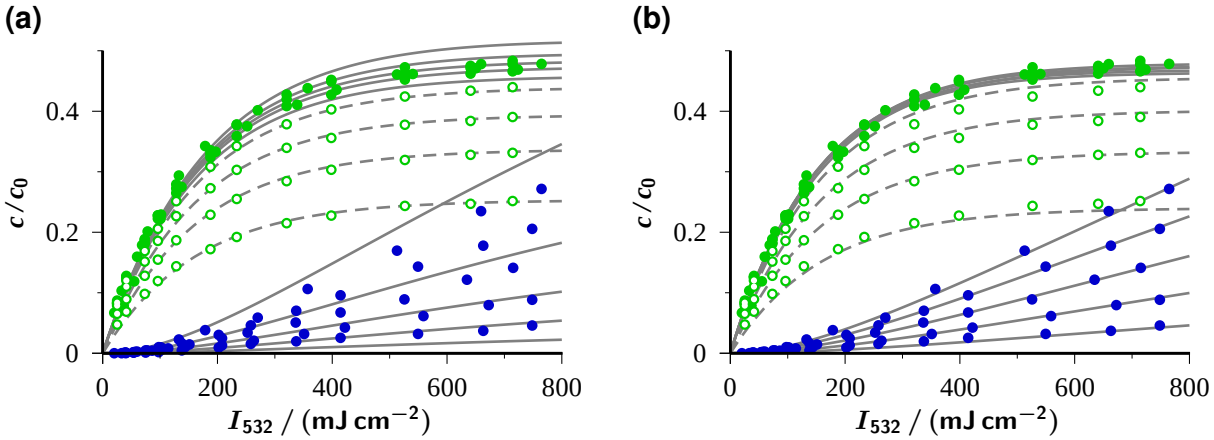

Supplementary Figure 4: Simultaneous best fits to the experimental concentration and intensity dependences (data from Figure 3a of the main paper) obtained with the closed-form solutions for very short-lived (a) and very long-lived (b) ^{3}SCRP. Best-fit parameters (for the kinetic scheme, see Supplementary Figure 3) with the effective laser pulse duration T and with the intensities I_{532} specified in mJ cm^{-2}: (a), $k_{\mathrm{exc}}T = 6.2 \times 10^{-3} I_{532}$, $k_{\mathrm{d}}T = 5.1 \times 10^{-3}$, $k_{\mathrm{q}}T = 14\,\mathrm{M}^{-1}$, $\eta = 0.47$, $k_{\mathrm{ion}}T = 2.3 \times 10^{-3} I_{532}$; (b), $k_{\mathrm{exc}}T = 6.4 \times 10^{-3} I_{532}$, $k_{\mathrm{d}}T = 2.0 \times 10^{-2}$, $k_{\mathrm{q}}T = 42\,\mathrm{M}^{-1}$, $\eta = 0.50$, $k_{\mathrm{ion}}T = 5.6 \times 10^{-4} I_{532}$. For further explanation, see text.

2.3 Thermal reaction between Asc^{2-} and the irradiated catalyst

Supplementary Figure 5 demonstrates that the addition of Asc^{2-} after exhaustive illumination of the catalyst Rubpy (in the absence of Asc^{2-}) leads to formation of the same species as the illumination in the presence of the catalyst. Because there are no spectral contributions from other species, the maximum appears slightly red shifted compared to that in Figure 5b of the main paper.

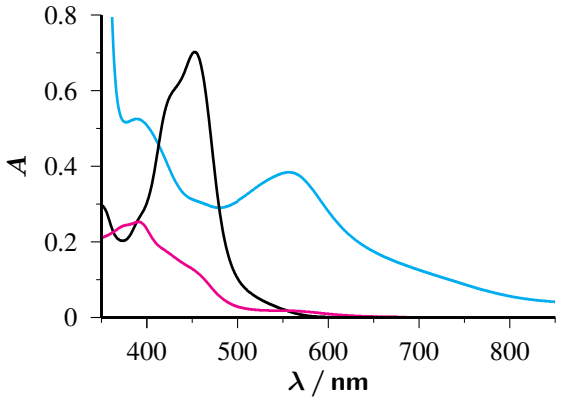

Supplementary Figure 5: Absorption spectra of the starting catalyst Rubpy before (black) and after 532 nm laser illumination in the absence of Asc^{2-} (magenta), and of the species after subsequent addition of 50 mM Asc^{2-} (cyan). All other conditions as in Figure 5b of the main paper. For further information, see text.

3 Application-related details

3.1 Electron capture by ClPhAcA

ClPhAcA does not absorb in the UV-A. Hence, we were able to employ the very simple 355 nm-driven electron source investigated in Ref. 42 of the main paper to access $e_{aq}^{\bullet-}$ and scavenge it with ClPhAcA. The only difference to the electron generator of the present work is the omission of Rubpy and the shorter operating wavelength; apart from that, Asc^{2-} is used in the same way, at a similar concentration, and at identical pH (12.65).

Supplementary Figure 6 displays a Stern–Volmer series of experiments with variation of the ClPhAcA concentration, which gives a rate constant of $5.0 \times 10^8\,M^{-1}s^{-1}$. The identical concentrations of $e_{aq}^{\bullet-}$ directly after the laser flash, regardless of the ClPhAcA concentration, establish that ClPhAcA only scavenges the liberated $e_{aq}^{\bullet-}$.

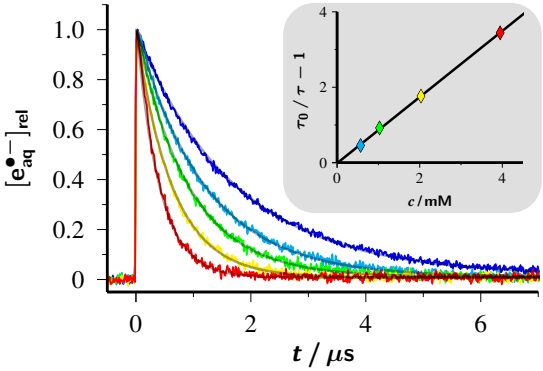

Supplementary Figure 6: Scavenging of $e_{aq}^{\bullet-}$ by ClPhAcA. Shown are concentration traces for $e_{aq}^{\bullet-}$, normalized to the maximum in the absence of ClPhAcA. Electron generator, 5 mM aqueous Asc^{2-} (pH 12.65) driven by 355 nm laser pulses. ClPhAcA concentrations (colour code), 0 mM (black), 0.5 mM (blue), 1 mM (green), 2 mM (yellow), 4 mM (red). The traces have been overlaid with best-fit functions of type exp $\left[-t/\tau\right]$. Inset, Stern–Volmer plot based on the lifetimes τ of the main plot, same colour code as there. τ_0 is the lifetime in the absence of ClPhAcA. Further explanation, see text.